# An Improved Model Based on UTD for Multiple Diffractions by Buildings

## Reza Arablouei<sup>1</sup>, Ayaz Ghorbani<sup>2</sup>

M.Sc. Student of Faculty of Electrical Engineering, Amirkabir University of Technology.
 Assis. Prof. of Faculty of Electrical Engineering, Amirkabir University of Technology.

## P. O. Box 15875-4413, Tehran, Iran a7923221@aut.ac.ir

Abstract - In this paper, a new propagation model based on UTD for multiple diffraction paths in cellular mobile radio communications in urban environments is proposed. Moreover, the most rigorous novel UTD-based expressions for multiple diffractions by buildings and excess path losses are drived and analyzed. For this purpose, building rows are supposed to have rectangular cross-sections with the same heights and spacings. In addition, in this analysis actual electrical properties of buildings are regarded. Previous studies have been concentrated on the simplified models that approximated building rows as absorbing half-screens or perfectly conducting half-screens (knife-edges) or 90 degrees wedges. In this work, buildings are assumed flat-roofed parallel rows of dielectric blocks and their actual relative permittivity and conductivity are applied.

**Keywords:** Urban radio propagation, multiple building diffractions, excess path loss, uniform theory of diffraction, land mobile radio cellular systems

### 1- Introduction

Introducing a high quality service of cellular mobile telephone and other relative radio facilities has been known as an important objective for modern telecommunication industries and many researchers have dealt with it. Radio signal characteristics force fundamental limits on the design and performance of the cellular mobile communication systems. Particularly, in urban environments high density of buildings greatly influences radio signal characteristics. Therefore, without considering effects of buildings on radio wave propagation in the urban environments, an accurate prediction of path loss and coverage area will not be accessible. If more rigorous model is used for buildings, more precise prediction will be available.

Many studies have been carried out for invetigating radio wave propagation over multiple buildings [1-10] Primary efforts were physicaloptics-based approaches which employed physical optics theorem and followed a simple concept, but were not adequately suitable for numerical calculations [1, 2]. Walfisch and Bertoni considered that outside of high-rise urban core, a city's buildings are of nearly uniform heights and spacings and are organized by street systems into rows. They approximated the rows of buildings as absorbing half-screens, so that radio wave propagation was a process as multiple forward diffractions over half-screens [1]. Saunders and Bonar gave an explicit solution to the Walfisch and Bertoni's problem, where attenuation function was derived in terms of special functions [3] and then they extended their solution for buildings of irregular heights and spacings [4, 5]. Neve and Rowe solved the multiple diffractions over buildings for the first time using UTD-based propagation model [6]. Zhang simplified Neve and

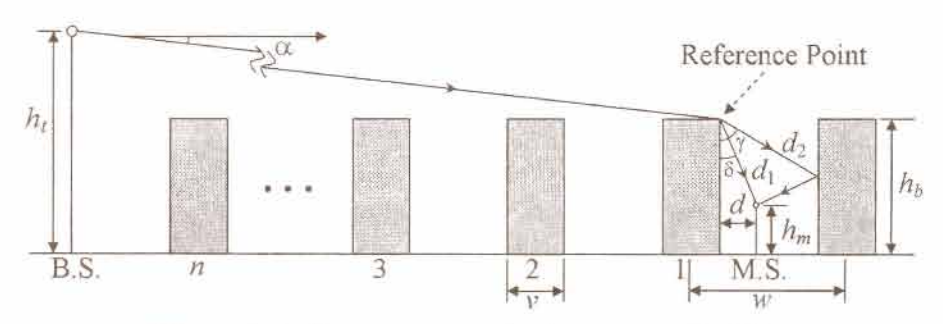


Figure 1 Radio wave propagation in presence of buildings

Rowe's formulation [7] and developed it including wide-band characteristics of the environment [8]. Juan-Llácer and Cardona produced a new solution in terms of UTD diffraction coefficients [9] using a straightforward technique based on the final solution for the attenuation function for multiple edges given in [2]. Finally, Kara and Yazgan have improved Zhang's model by using finitely conducting wedges of angle  $\pi/2$  for modeling building rows instead of perfectly conducting half-screens (knife-edges) [10]. Kara and Yazgan's initiative is very considerable, because their model is very close to reality, at least in some European countries like Turkey (Kara and Yazgan's country) that most of the buildings have wedge-type roofs outside the high-rise urban core. In the new model proposed in this paper, the propagation environment has been assumed as in previous works, except that cross-sections of building rows are considered rectangular, as shown in Figure 1. This assumption makes fundamental differences from traditional scenarios. which suppose each building to contain only one diffracting edge. In the new model, each building has two diffracting edges, so that previously derived expressions for multiple building diffraction attenuation are not usable here. Therefore, a novel expression for loss of multiple diffractions by buildings based on the new model is derived. Then, a new formulation for the received electric field intensity at the mobile station located at the local street level is derived and the excess path loss is achieved using it. The results obtained from the new model are compared with results of the previous models and existing measurements. Convincing improvements are attained.

## 2 - Derivation

## 2.1 Multiple building diffraction attenuation

The path loss contribution due to multiple diffractions by buildings is defined as

$$L_{MBD} = -20log_{10} \left( \frac{E_n}{E_0} \right) \tag{1}$$

where  $E_0$  is the transmitted field and  $E_n$  is the received electric field intensity at the reference point with n existing building rows. Reference point is defined just on top of the last wall close to the mobile station as in Figure 1. In order to predict the multiple building diffraction loss, we have to find out the received electric field intensity at the reference point.

To do so, all rays launched from the transmitter and arrived at the reference point are determined and each field intensity contribution is evaluated. Then, all of the contributions are summed up. Figure 2 shows all possible rays, which can contribute to the received signals at the reference point and mobile station.

Assuming n building rows and according to the mentioned reason and following a procedure similar to [7], the received field normalized to the transmitted field  $E_0$  can be written as

$$\frac{E(n)}{E_0} = e^{-jk[\nu + (n-1)w]\cos(\alpha)} + D_1 e^{-jk[\nu + (n-1)w\cos(\alpha)]} 
+ D_2 D_3 e^{-jk(w + [(n-2)w + \nu]\cos(\alpha))} 
\cdot \left(1 + \sum_{i=3}^n D_5^{i-2} e^{-jk(i-2)w[1-\cos(\alpha)]}\right) 
+ D_4 D_3 e^{-jk(w + \nu + (n-2)w\cos(\alpha))} 
\cdot \left(1 + \sum_{i=3}^n D_5^{i-2} e^{-jk(i-2)w[1-\cos(\alpha)]}\right)$$
(2)

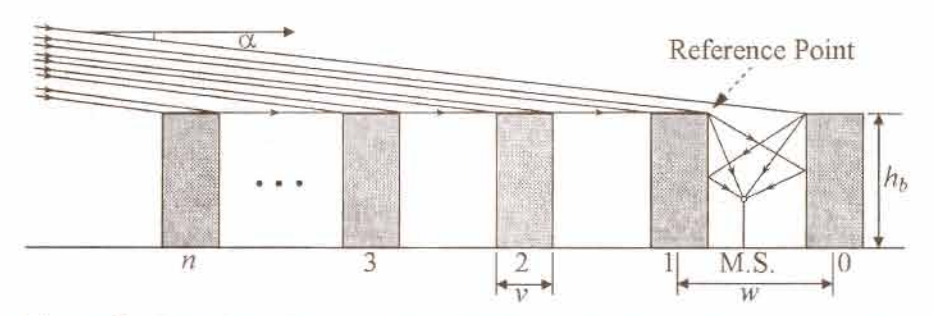


Figure 2 Illustration of all rays contributing to the received signal received signa

As we know:

$$\sum_{m=0}^{n-1} z^m = \frac{1-z^n}{1-z} \tag{3}$$

and applying some simplifications, we have

$$\begin{split} \frac{E(n)}{E_0} &= e^{-jk[\nu + (n-1)w \cdot \cos(\alpha)]} \Big( D_1 + e^{-jk\nu[\cos(\alpha) - 1]} \Big) \\ &+ D_3 e^{-jk[w(1 + (n-2)\cos(\alpha)) + \nu]} \\ &\cdot \Big( D_4 + D_2 e^{-jk\nu[\cos(\alpha) - 1]} \Big) \\ &\cdot \left( \frac{1 - \Big( D_5 e^{-jkw[1 - \cos(\alpha)]} \Big)^{n-1}}{1 - D_5 e^{-jkw[1 - \cos(\alpha)]}} \right) \end{split} \tag{4}$$

where v is the width of the individual building row, w is the spacing of the building rows, and  $\alpha$  is the incident plane wave's angle with the horzon (see Figures 1, 2).

We define  $D_1$  as

$$D_1 = D\left(\varphi = \frac{3\pi}{2}, \varphi' = \alpha + \frac{\pi}{2}, L = \nu, \beta_0 = \frac{\pi}{2}\right) \cdot \frac{1}{\sqrt{\nu}}$$
 (5)

where  $D(\varphi, \varphi; L, \beta_0)$  is the diffraction coefficient for a finitely conducting wedge of angle  $\pi 2$  and  $1/\sqrt{\nu}$  is the spreading factor [11]. Geometry depicting the single diffraction event and trajectory of related ray corresponding to  $D_1$  is shown in Figure 3.

In order to evaluate the diffraction coefficient for a finitely conducting wedge, we use Luebbers's heuristic coefficient, which includes a special care for grazing incidence case [12]:

$$D = \frac{-e^{-j\frac{\pi}{4}}}{2n\sqrt{2\pi k}\sin(\beta_0)}$$

$$\cdot \left\{ G_0 \left[ \cot\left(\frac{\pi - (\phi - \phi')}{2n}\right) F(kLa^-(\phi - \phi')) + R_0 \cot\left(\frac{\pi - (\phi + \phi')}{2n}\right) F(kLa^-(\phi + \phi')) \right] + G_n \left[ \cot\left(\frac{\pi + (\phi - \phi')}{2n}\right) F(kLa^+(\phi - \phi')) + R_n \cot\left(\frac{\pi + (\phi + \phi')}{2n}\right) F(kLa^+(\phi + \phi')) \right] \right\}$$

where  $G_0$  and  $G_n$  are the gain factors defined to generalize the formulation to include the grazing incidence case [12]:

$$G_0 = \begin{cases} 1/(1+R_0) & \varphi' = 0, & |1+R_0| > 0 \\ 1/2 & \varphi' = n\pi \\ 1 & otherwise \end{cases}$$
 (7)

$$G_{n} = \begin{cases} 1/(1+R_{n}) & \phi' = n\pi & |1+R_{n}| > 0 \\ 1/2 & \phi' = 0 \\ 1 & otherwise \end{cases}$$
 (8)

where  $R_0$  and  $R_n$  are the reflection coefficients for proper polarization for the zero-face with incident angle of  $\varphi$ ?and for the n-face with reflection angle of  $n\pi$ - $\varphi$ , respectively.

The function F is the Fresnel transition function [11]:

$$F(x) = 2j\sqrt{x}e^{jx} \int_{-\pi}^{\infty} e^{-jt^2} d\tau$$
 (9)

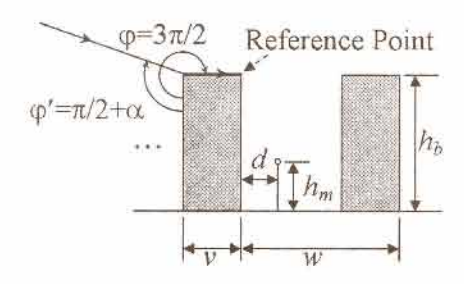


**Figure 3** Geometry depicting single diffraction event and trajectory of related ray corresponding to  $D_1$ 

and L is the distance parameter:

$$L = \frac{ss'\sin^2\beta_0}{s+s'} \tag{10}$$

also

$$a^{\pm}(\beta) = 2\cos^2\left(\frac{2nN^{\pm} - \beta}{2}\right), \qquad \beta = \varphi \pm \varphi' \quad (11)$$

where  $N^+$  and  $N^-$  are the integers, which most closely satisfy the equations:

$$2n\pi \cdot N^+ - \beta = \pi$$

$$2n\pi \cdot N^- - \beta = -\pi$$

Referring to Figures 4 and 5 and following the same rationale,  $D_2$  and  $D_3$  are written as

$$D_{2} = D\left(\phi = \pi, \phi' = \alpha, L = w - v, \beta_{0} = \frac{\pi}{2}\right) \cdot \frac{1}{\sqrt{w - v}}$$

$$D_{3} = D\left(\phi = \frac{3\pi}{2}, \phi' = \frac{\pi}{2}, L = \frac{v(w - v)}{w}, \beta_{0} = \frac{\pi}{2}\right) \cdot \frac{1}{\sqrt{v}}$$
(13)

Diffracting Wedge  $\phi=3\pi/2$   $\phi'=\pi/2$   $h_b \dots$ 

Figure 5 As Figure 3 for  $D_3$ 

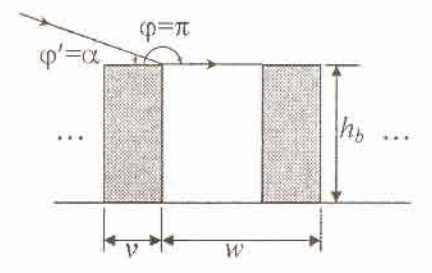


Figure 4 As Figure 3 for D2

Moreover,  $D_4$  is defined as

$$D_4 = \left(D_a D_b - \frac{1}{2jkv} \frac{\partial D_b}{\partial \varphi'} \frac{\partial D_a}{\partial \varphi}\right) \cdot \frac{1}{\sqrt{v}} \cdot \frac{1}{\sqrt{w-v}}$$
(14)

where

$$D_a = D\left(\phi = \frac{3\pi}{2}, \phi' = \alpha + \frac{\pi}{2}, L = \nu, \beta_0 = \frac{\pi}{2}\right)$$
 (15)

$$D_b = D\left(\varphi = \pi, \varphi' = 0, L = \frac{v(w - v)}{w}, \beta_0 = \frac{\pi}{2}\right)$$
 (16)

In fact,  $D_a D_b - \frac{1}{2jkv} \frac{\partial D_b}{\partial \phi'} \frac{\partial D_a}{\partial \phi}$  is the double

diffraction coefficient by two consecutive wedges

of angle  $\pi 2$  (See Figure 6), also  $D_a$  and  $D_b$  are the first-order diffraction coefficients of the first and second wedges, respectively. Incident field to the second wedge (diffracted from the first wedge)

First Diffracting Wedge Second Diffracting Wedge  $\phi_1' = \pi/2 + \alpha$   $\phi_2' = 0$   $\phi_2' = 0$  ...

Figure 6 Geometry depicting double diffraction event and trajectory of related ray corresponding to  $D_4$ 

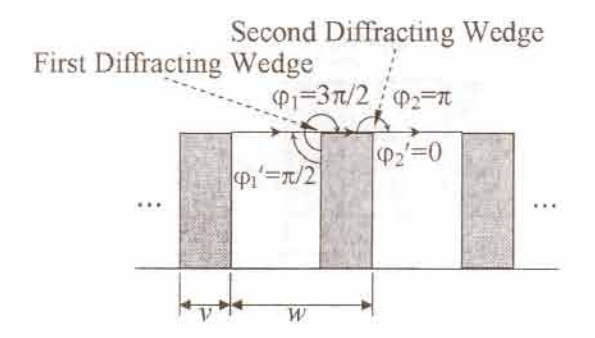


Figure 7 As Figure 6 for D<sub>5</sub>

arrives at grazing incidence ( $\phi$ ?=0), so slope diffraction component must be taken into account [12, 13]. Namely, the term  $-\frac{1}{2jkv}\frac{\partial D_b}{\partial \phi'}\frac{\partial D_a}{\partial \phi}$  rep-

resents the slope diffraction contribution to the double diffraction event [12, 13].

To clarify the discussion, we assume that the field incident on the first wedge has a slow spatial variation. Hence, we can provide the expression for the doubly diffracted field in a generalized form as

$$E_1^d = E_2^i = E_1^i D_a A(s', v) e^{-jkv}$$
(17)

for the field diffracted by the first wedge and incident on the second edge, and

$$E_{2}^{d} = \left[ E_{2}^{i} D_{b} + \frac{1}{2jk} \frac{\partial D_{b}}{\partial \varphi'} \frac{\partial E_{2}^{i}}{\partial u_{2}} \right] A(s, s', v) e^{-jks}$$
(18)

for the field diffracted by the second wedge that can be simplified using

$$\frac{\partial E_2^i}{\partial u_2} = E_1^i A(s', v) e^{-jkv} \frac{\partial D_a}{\partial \varphi} \left(\frac{1}{-v}\right)$$
 (19)

 $E_2^d = D_4 E_1^i A(s', v) A(s, s', v) e^{-jk(s+v)}$  (20)

Hence,  $1/\sqrt{v}$  and  $1/\sqrt{w-v}$  in (14) are the spreading factors for diffraction events taken place at the first and second wedges (A(s',v) and,(A(s,s',v) respectively (see Figure 6).

In a similar manner,  $D_5$  is given by

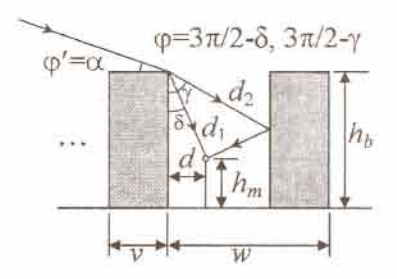


Figure 8 Geometry depicting single diffraction events and trajectories of related rays corresponding to  $D_6$ 

$$D_{5} = \left(D_{c}D_{d} - \frac{1}{2jkv}\frac{\partial D_{d}}{\partial \varphi'}\frac{\partial D_{c}}{\partial \varphi}\right) \cdot \frac{1}{\sqrt{v}} \cdot \frac{1}{\sqrt{w-v}}$$
(21)

where

$$D_{c} = D\left(\phi = \frac{3\pi}{2}, \phi' = \frac{\pi}{2}, L = \frac{v(w - v)}{w}, \beta_{0} = \frac{\pi}{2}\right)$$

$$D_{d} = D\left(\phi = \pi, \phi' = 0, L = \frac{v(w - v)}{w}, \beta_{0} = \frac{\pi}{2}\right)$$
(22)

That is,  $D_5$  is defined similar to  $D_4$  with only a difference at the incident ray to the first wedge launched from last caustic point (see Figure 7). Geometries depicting single or double diffraction events and trajectories of related rays corresponding to each  $D_2$  to  $D_5$  are shown in Figures 4 to 7.

## 2.2 - Path loss prediction

The path loss is the summation of the excess and free space path losses. The free space path loss is well known and easy to evaluate, also the excess path loss can be calculated by adding the multiple building diffraction loss  $L_{MBD}$  to the local building diffraction loss.

In this paper, we prefer to derive a separate expression for the excess path loss instead of adding two abovementioned losses. Since, we found out that predicting the local building diffraction loss in a separate process will not conclude a very precise prediction of the excess path loss. In doing so, the received electric field intensity at the mobile station location is found, and then the excess path loss is determined due to the received field's

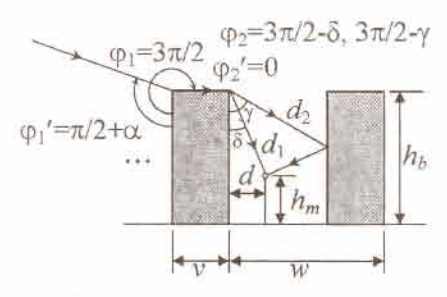


**Figure 9** Geometry depicting double diffraction events and trajectories of related rays corresponding to  $D_7$ 

In our scenario shown in Figure 1, the received electric field intensity at the mobile station can be evaluated in a manner similar to previous subsection. In fact, propagation process for the arrived rays at the mobile station is similar to those arrive at the reference point, except suffering an extra diffraction event from the reference point toward the mobile station at the local street level. Addtionally, opposite building row can cause reflected rays reaching to the mobile station. Thus, the normalized received field at the mobile station is achieved as

$$\begin{split} \frac{E^{m}(n)}{E_{0}} &= e^{-jk\left[v + (n-1)w \cdot cos(\alpha)\right]} \Big(D_{7} + D_{6}e^{-jkv\left[cos(\alpha) - 1\right]}\Big) \\ &+ D_{8}e^{-jk\left(w\left[1 + (n-2)cos(\alpha)\right] + v\right)} \\ &\cdot \Big(D_{4} + D_{2}e^{-jkv\left[cos(\alpha) - 1\right]}\Big) \\ &\cdot \left(\frac{1 - \Big(D_{5}e^{-jkw\left[1 - cos(\alpha)\right]}\Big)^{n-1}}{1 - D_{5}e^{-jkw\left[1 - cos(\alpha)\right]}}\right) \end{split}$$

where  $D_6$  to  $D_8$  are expressed as  $D_6 = D\left(\varphi = \frac{3\pi}{2} - \delta, \varphi' = \alpha, L = d_1, \beta_0 = \frac{\pi}{2}\right)$   $\cdot \frac{1}{\sqrt{d_1}} e^{-jkd_1}$   $+ D\left(\varphi = \frac{3\pi}{2} - \gamma, \varphi' = \alpha, L = d_2, \beta_0 = \frac{\pi}{2}\right)$   $\cdot \frac{1}{\sqrt{d_2}} e^{-jkd_2} \cdot R(\gamma)$ (25)

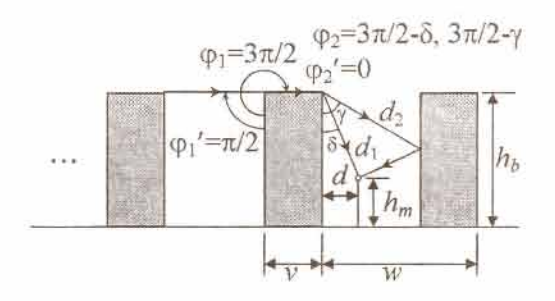


Figure 10 As Figure 9 for D<sub>8</sub>

$$D_{7} = \left(D_{e}D_{x} - \frac{1}{2jkv}\frac{\partial D_{x}}{\partial \varphi'}\frac{\partial D_{e}}{\partial \varphi}\right) \cdot \frac{1}{\sqrt{v}} \cdot \frac{1}{\sqrt{d_{1}}}e^{-jkd_{1}}$$

$$+ \left(D_{e}D_{y} - \frac{1}{2jkv}\frac{\partial D_{y}}{\partial \varphi'}\frac{\partial D_{e}}{\partial \varphi}\right)$$

$$\cdot \frac{1}{\sqrt{v}} \cdot \frac{1}{\sqrt{d_{2}}}e^{-jkd_{2}} \cdot R(\gamma)$$

$$D_{8} = \left(D_{f}D_{x} - \frac{1}{2jkv}\frac{\partial D_{x}}{\partial \varphi'}\frac{\partial D_{f}}{\partial \varphi}\right) \cdot \frac{1}{\sqrt{v}} \cdot \frac{1}{\sqrt{d_{1}}}e^{-jkd_{1}}$$

$$+ \left(D_{f}D_{y} - \frac{1}{2jkv}\frac{\partial D_{y}}{\partial \varphi'}\frac{\partial D_{f}}{\partial \varphi}\right)$$

$$\cdot \frac{1}{\sqrt{v}} \cdot \frac{1}{\sqrt{d_{2}}}e^{-jkd_{2}} \cdot R(\gamma)$$

where

(24)

$$D_e = D\left(\varphi = \frac{3\pi}{2}, \varphi' = \alpha + \frac{\pi}{2}, L = \nu, \beta_0 = \frac{\pi}{2}\right)$$
 (28)

(27)

$$D_f = D\left(\phi = \frac{3\pi}{2}, \phi' = \frac{\pi}{2}, L = \frac{v(w - v)}{w}, \beta_0 = \frac{\pi}{2}\right)$$
(29)

$$D_x = D\left(\varphi = \frac{3\pi}{2} - \delta, \varphi' = 0, L = d_1, \beta_0 = \frac{\pi}{2}\right)$$
 (30)

$$D_y = D\left(\varphi = \frac{3\pi}{2} - \gamma, \varphi' = 0, L = d_2, \beta_0 = \frac{\pi}{2}\right)$$
 (31)

Geometries depicting single or double diffraction

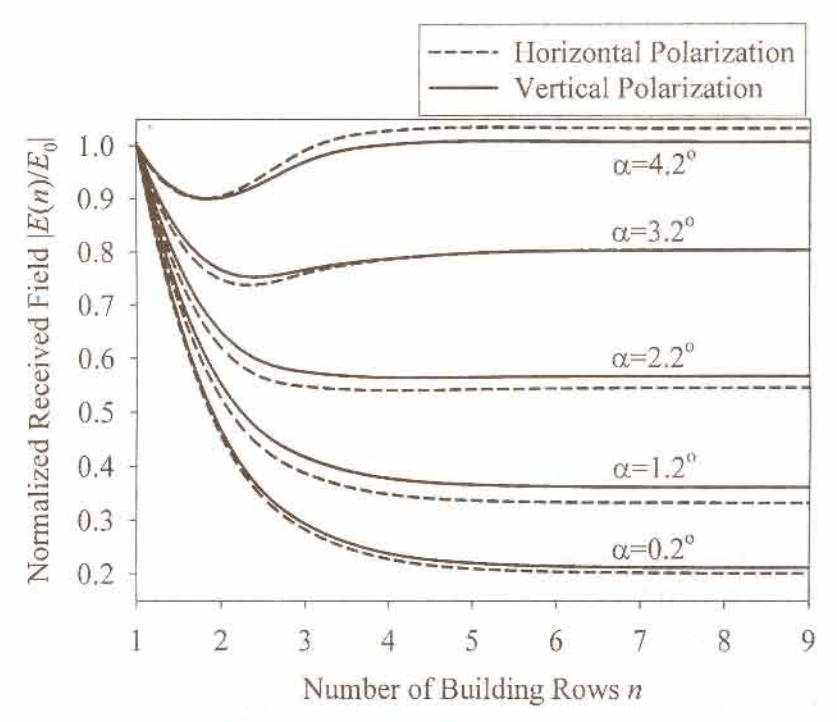


Figure 11 The normalized total electric field intensity at the reference point versus number of building rows for both vertically and horizontally polarized electric fields. Here, f=922 MHz, w =50 $\lambda$ , v=28 $\lambda$ ,  $\epsilon_r$ =5.5, and  $\sigma$  = 0.023 S/m

events and trajectories of related rays corresponding to each  $D_6$  to  $D_8$  are shown in Figures 8 to 10; also, the parameters  $d_1$ ,  $d_2$ ,  $\delta$ , and  $\gamma$  are shown in these Figures.

Moreover,  $1/\sqrt{d_1}$  and  $1/\sqrt{d_2}$  are the spreading factors for diffracted rays from the reference point toward the mobile station;  $1/\sqrt{d_1}$  is for the direct ray and  $1/\sqrt{d_2}$  is for the ray reflected from the opposite building row.

Second terms of  $D_6$  to  $D_8$  are multiplied by  $R(\gamma)$ , which is the reflection coefficient of the reflecting wall for proper polarization.

It is evident that the definition of  $D_8$  is similar to  $D_7$  with only a difference at incident ray to the first wedge launched from last caustic point (see Figure 10).

The excess path loss is given by

$$L_{Excess} = -20log_{10} \left( \frac{E_n^m}{E_0} \right)$$
 (32)

where  $E_n^m$  and  $E_0$  represent the received field at the mobile station with n existing building rows and the transmitted field, respectively.

### 3 - Results and discussion

The normalized total electric field intensity at the reference point versus number of existing building rows n is shown in Figure 11 for f=922 MHz,  $w=50\lambda$ ,  $v=28\lambda$ ,  $\varepsilon_r=5.5$ , and  $\sigma=0.023$  S/m for both vertically and horizontally polarized electric fields. Applied relative permittivity and conductivity for the diffracting and reflecting building facades in the simulation are very close to the actual electrical properties of the typical urban buildings [13, 14]. In Figure 11, the angle of incidence a is a parameter. Moreover, the solid and dashed lines are for the vertically and horizontally polarized fields, respectively. It is expected that  $|E(n)/E_0|$  is settled in a fixed value of less than 1 for α? 3.2° [6, 7]. Specifically, it depends less on the polarization. Moreover, it can happen that  $|E(n)/E_0| > 1$  at  $\alpha > 4.2^\circ$ . It can be understood there is a critical angle between 3.2° and 4.2°. This confirms results of the previous studies [6].

We do not consider the case of  $\alpha$ <0°, which implies that the base station transmitting antenna is erected below the building rooftop levels. This is not the case of interest amplitude.

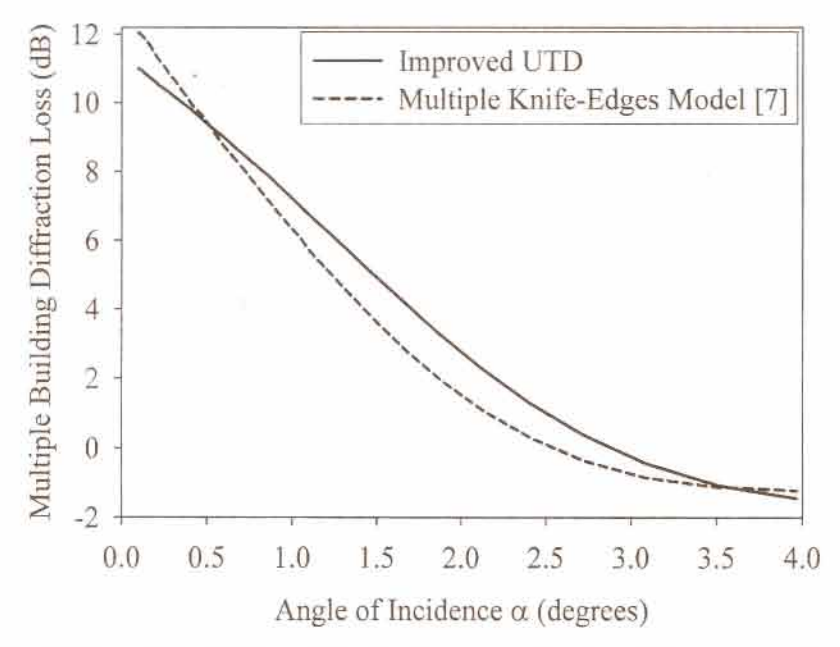


Figure 12 The settled multiple building diffraction loss versus the angle of incidence Jpredicted by the new model and the traditional multiple knife-edges model [7]. Here f=922 MHz, f=922 MHz,

in this paper. Since, in this situation, the prominent process of propagation is not the multiple diffractions over the building rooftops. On the contrary, reflections and diffractions from lateral building facades and corners are the most contributing phenomena at the propagation when  $\alpha$ <0°.

Consecutive diffractions reduce the transmitted field by a ray abruptly. That is why, rays that suffer several diffraction events are not able to contribute to the received field significantly. The implication of this fact is that the multiple building diffraction loss will be saturated when the number of building rows exceeds a certain quantity. Of course, we take into account all possible rooftop multiple diffractions in our model.

In Figure 12, the settled multiple building diffraction loss (for a large number of building rows) is plotted versus  $\alpha$  using both the new model and the traditional multiple knife-edges model [7]. Here, f=922 MHz, w=35 m, and v=21 m. It should be pointed out that although Kara and Yazgan [10] have introduced a more realistic model as compared to the multiple knife-edges model, their

model predicts the multiple building diffraction loss not very different from Zhang's one [7].

As observed in Figure 12, when the angle of incidence  $\alpha$  increases, buildings occlude the radiated fields less and this is the case that diffracted rays from building rooftops can be aggregated constructively. Hence, it is prsumable to have negative multiple building diffraction loss with such values of  $\alpha$  greater than 3°.

The excess path loss is drawn versus  $\alpha$  in Figure 13, for f=922 MHz, w=35 m, v=21 m, d=4.5 m,  $h_b$ =12 m, and  $h_m$ =3 m. As shown in Figure 1, d is the distance between the mobile station and the last diffracting wall; also  $h_b$  and  $h_m$  are the mean height of the buildings and the mobile station height. Figure 13, includes predictions by Zhang's model [7] for the same values of parameters, too. It is noteworthy that Kara and Yazgan [10] have applied Zhang's approximate expression for the local building diffraction loss [8]. Therefore, since their model predicts the same multiple building diffraction loss as Zhang's one, the excess path loss predicted by their model will be the same as Zhang's one too.

Comparing the two different sorts of the results

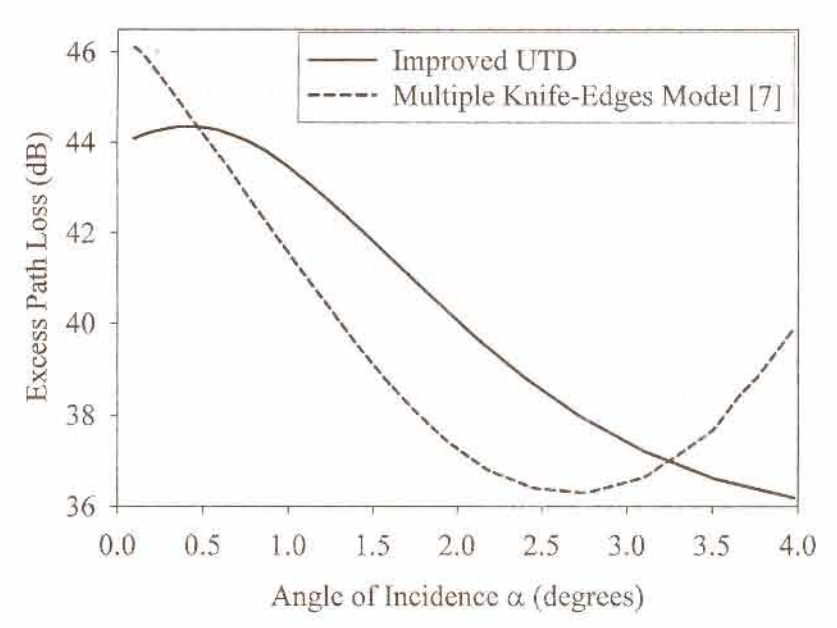


**Figure 13** The excess path loss versus α predicted by the new model and the multiple knife-edges model [7]. Here, f=922 MHz, w=35 m, v=21 m,  $\varepsilon_r$ =5.5,  $\sigma$ =0.023 S/m, d=4.5 m,  $h_b$ =12 m, and  $h_m$ =3 m

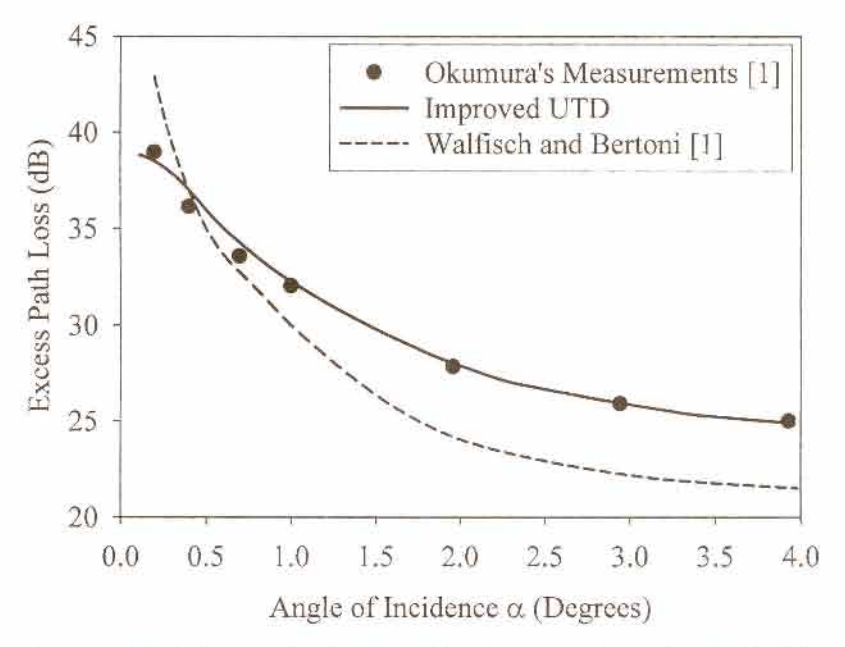


**Figure 14** The excess path loss versus α predicted by the new model and a physical-optics-based model of Walfisch and Bertoni guoted there in along with Okumura's measurements [1] for f=922 MHz, w=40 m, v=25 m,  $\varepsilon_r$ =5.5,  $\sigma$ =0.023 S/m, d=5 m,  $h_b$ =15 m, and  $h_m$ =1.8 m

shows that the new improved UTD-based model provides predictions that are more acceptable. As we can observe in Figure 13, more rational and explainable predictions are available using the new proposed model. For instance, there is a pesimistic rising deviation in the predicted excess

path loss curve by Zhang's model [7] at  $\alpha$ >2.7°, whereas new model's predictions do not possess such erroneous behavior.

The excess path loss versus a predicted by the new model and the physical-optics-based model of Walfisch and Bertoni [1] is shown in Figure 14 for f=922 MHz, w=40 m, v=25 m, d=5 m,  $h_b$ =15 m, and  $h_m$ =1.8 m. Additionally, some measured data treated by Okumura [1] are compared in Figure 14.

Examining Figure 14, one can conclude that the new model's predictions excellently fit the measurement data. Moreover, it makes evident how considering building rows as absorbing half-screens (Walfisch and Bertoni [1]) can cause errors of prediction.

All of these improvements can be explained due to using more realistic model for buildings and taking into account slope diffraction, which is a higher-order term of diffraction. As well, considering building rows as dielectric blocks with relative permittivity and conductivity equal to the mean actual relative permittivity and conductivity of the typical urban buildings is more appropriate than considering as absorbing half-screens or per-

fectly conducting half-screens.

#### 4 - Conclusion

A UTD-based propagation model for predicting path loss in urban cellular mobile environments has been developed. This new model provides the novel rigorous expressions for the multiple diffractions by buildings and excess path losses, which make available more precise prediction for the path loss in urban mobile environments. Moreover, the new expressions are so appropriate for numerical calculation. Conclusively, this new model can be used for predicting the path loss, coverage area, intercellular interference, and other propagation characteristics for cellular mobile radio communication systems in urban, suburban, and rural environments.

#### 5- References

- J. Walfisch and H. L. Bertoni, "A theoretical model of UHF propagation in urban environments," *IEEE Transactions on Antennas* and Propagation, vol. 36, pp. 1788-1796, Dec. 1988.
- [2] L. E. Vogler, "An attenuation function for multiple knife-edge diffraction," *Radio Science*, vol. 17, no. 6, pp. 1541-1546, Nov./Dec. 1982.
- [3] S. R. Saunders and F. R. Bonar, "Explicit multiple building diffraction attenuation function for mobile radio propagation," *Electronics Letters*, vol. 27, no. 14, pp. 1276-1277, July 4, 1991.
- [4] S. R. Saunders and F. R. Bonar, "Prediction of mobile radio wave propagation over buildings of irregular heights and spacings," *IEEE Transactions on Antennas and Propa*gation, vol. 42, pp. 137-143, Feb. 1994.
- [5] Saunders, S.R., and Bonar, F.R., "Building diffraction modeling for area coverage prediction in mobile radio propagation," in Proceedings of IEE colloquium on diffraction modeling techniques embracing surface feature data, vol. 4, pp. 1-3, 1990.
- [6] M. J. Neve and G. B. Rowe, "Contributions toward the development of a UTD-based model for cellular radio propagation prediction," Proceedings of IEE on Microwave Antennas and Propagation, vol. 141, no. 5, pp. 407-414, Oct. 1994.
- [7] W. Zhang, "A more rigorous UTD-based expression for multiple diffractions by buildings," *Proceedings of IEE on Microwave Antennas and Propagation*, vol. 142, no. 6, pp. 481-484, Dec. 1995.
- [8] W. Zhang, "A wide-band propagation model based on UTD for cellular mobile radio communications," *IEEE Transactions on Antennas and Propagation*, vol. 45, pp. 1669-1678, Nov. 1997.
- [9] L. Juan-Llácer and N. Cardona, "UTD solution for the multiple building attenuation function for mobile radio wave propagation," Electronics Letters, vol. 33, no. 1, pp. 92-93, Jan. 2, 1997.
- [10] A. Kara and E. Yazgan, "UTD-based propagation model for the path loss characteristics

- of cellular mobile communications system," in *Proceedings of IEEE antennas and propagation society symposium*, pp. 392-395, 1999.
- [11] R. G. Kouyoumjian and P. H. Pathak, "A uniform geometrical theory of diffraction for an edge in a perfectly conducting surface," *Proceedings of IEEE*, vol. 62, no.11, pp. 1448-1461, Nov. 1974.
- [12] R. J. Luebbers, "A heuristic UTD slope diffraction coefficient for rough lossy wedges," *IEEE Transactions on Antennas and Prop*gation, vol. 37, pp. 206-211, Feb. 1989.
- [13] Zhang, H., Yoshino, T., Ito, S., and Nagasawa, Y., "A UTD-based Approach to predicting diffraction by buildings for cellular mobile communication," in *Proceedings of IEEE-APS conference on antennas and propagation for wireless communication*, pp.13-16, 1998.
- [14] Lawton, M.C., and McGeehan, J.P., "The application of a deterministic ray launching algorithm," *IEEE Transactions on Vehicular Technology*, vol. 43, pp. 955-969, Nov., 1994.